



Experimental investigation on erosion progression and strength reduction of gap-graded cohesionless soil subjected to suffusion

Yue Liang^{1,2} · Bin Zhang² · Yongmei Yang³ · Hongjie Zhang² · Lei Dai²

Received: 21 June 2022 / Accepted: 14 March 2023 / Published online: 24 March 2023
© The Author(s), under exclusive licence to Springer-Verlag GmbH Germany, part of Springer Nature 2023

Abstract

Suffusion is a typical mode of internal erosion that leads to the deterioration of earthen structures. A stress-controlled experimental apparatus has been developed, which is adopted to investigate the characteristics of the erosion process and strength reduction of gap-graded cohesionless soil subjected to suffusion. Experimental results reveal that the critical hydraulic gradient significantly relates to the relative content of fine and coarse particles. Besides, under the same stress condition, the suffusion process is divided into three typical stages, i.e., the steady seepage stage (S1), the suffusion initiation stage (S2), and the suffusion equilibrium stage (S3). The suffusion process and the responses of the soil strength are explored with a newly defined coefficient, i.e., erosion ratio (ER). The coefficient ER is defined as the percentage of the cumulative weight of the eroded fine particles to the initial fine particle content in the specimen. The experiment results reveal that when ER is smaller than 6%, the effect of particle erosion on the strength of the soil is negligible. Nevertheless, the strength reduction is remarkable if the ER continuously increases. When the ER reached 35%, the critical friction angle decreased by 12.04°, and the strength decreased by 27.38% compared with the intact specimen. Moreover, the internal stability assessment and fine particle migration characteristics of gap-graded cohesionless soil are further analyzed according to particle-size distribution criteria. The diversity of the strength reduction trend is attributed to the differences in soil skeleton structure.

Keywords Gap-graded cohesionless soil · Suffusion · Fine particle erosion · Strength reduction

Introduction

The internal erosion of soil is widely observed in both natural soil deposits and artificially engineered fill structures. This phenomenon is one of the most common causes of the reduction and failure of dams, tunnels, levees, etc. (Hu et al. 2020b; Masi et al. 2020; Zhou et al. 2020a). The erosion will lead to a significant change in the physical and geo-mechanical properties of the soils (e.g., the hydraulic conductivity, the shear strength, the void ratio, etc.) (Liang et al. 2017a; Mehdizadeh et al. 2017). In the current studies, four forms

of internal erosion have been classified, i.e., concentrated leak erosion, backward erosion, contact erosion, and suffusion (Kodieh et al. 2021; Yang et al. 2019). Suffusion refers to the process by which fine particles are washed out of the soil matrix through the voids between the coarse particles by seepage force (Israr and Aziz 2019; Ke and Takahashi 2012). Suffusion leads to significant modifications in the hydraulic and mechanical characteristics of the soil. Such modifications of the porous medium will be the catalyst for significant instabilities at the real scale of hydraulic structures. The expansion of suffusion usually leads to on-site disorders (e.g., sinkholes, settlements, preferential flow paths, etc.) (Benamar et al. 2019; Bonelli 2012; Deng et al. 2018; Douglas et al. 2019).

Suffusion is a complex phenomenon involving the process of pore-water flow, fluidized particle migration, and the deformation of porous media. The onset and the evolution of suffusion are governed by various variable factors (Chen et al. 2021a; Liang et al. 2017a). These factors include the hydraulic characteristics (e.g., the seepage direction, the hydraulic gradient, the inflow velocity, etc.) (Zhou et al.

✉ Bin Zhang
zbin196@163.com

¹ National Engineering Research Center for Inland Waterway Regulation, Chongqing Jiaotong University, Chongqing 400074, China

² School of River and Ocean Engineering, Chongqing Jiaotong University, Chongqing 400074, China

³ Port and Waterway Design Institute of Jiangxi Province, Jiangxi 330000, China

2020b), the physical and the geometric characteristics of the soil (e.g., the initial porosity, the initial dry density, the particle-size distribution, the particle shape, etc.), and the stress state (Chen et al. 2021b; Da-lang et al. 2020). Many of these research have proposed various criteria for defining the onset of suffusion based on the force equilibrium of particles in the specimen (Liang et al. 2017a). These criteria include the critical hydraulic head, the critical hydraulic gradient, the critical seepage flow velocity, and the critical hydraulic shear stress (Ke and Takahashi 2012; Liang et al. 2017a; Perzmaier 2007; Skempton and Brogan 1994). However, one of the most concerning issues in these studies is the influence mechanism of various material properties and environmental factors on the critical hydraulic gradient when suffusion occurs (Luo and Huang 2020). Experimental results indicate that the critical hydraulic gradient depends on the properties of soil, such as the spatial distribution of fine fractions (Horikoshi and Takahashi 2015; Li et al. 2019), dry densities, and inter-particle rolling resistance (Liang et al. 2017b; Ma et al. 2018). In addition, the critical gradient is also closely related to the stress condition, the water temperature, and the seepage flow direction (Jiang and Guan 2020; Luo et al. 2019; Xiong et al. 2020). The experiments reveal that the greater the angle to the horizontal level is, the harder it is for suffusion to occur and continue. For the horizontal seepage-induced suffusion under controlled vertical stress, both initiation and failure hydraulic gradients increased with initial dry density and fines content (Deng et al. 2020). Moreover, the critical hydraulic threshold is subjected to scale effects and depends on the history of hydraulic loading (Marot et al. 2012; Rochim et al. 2017; Rousseau et al. 2020). Besides, the particle movement process is very sensitive to changes in initial soil porosity, particle polydispersity, and packing porosity (Huang et al. 2020; Ma et al. 2018).

Suffusion-induced fines loss can lead to redistributing of the forcing chains and rearranging of the soil particles, consequently altering the mechanical properties of the soils (Hu et al. 2020b). Along with the loss of the fine particles, suffusion may render a loose soil structure with increased porosity and hydraulic conductivity and leads to considerable volumetric deformation (Hu et al. 2020b; Ke and Takahashi 2014). More microscopic observations show that the void-filling rate between coarse particles decreases with the loss of particles, leading to rearrangement in the soil microstructure (Li et al. 2020). This mechanism further leads to changes in soil porosity and permeability (Hu et al. 2020a; Liang et al. 2019; Prasomsri and Takahashi 2020). Most importantly, suffusion also significantly affects the mechanical properties of eroded soils, and this topic has attracted the attention of various researchers (Chen et al. 2019; Ślusarek and Łupieżowiec 2021). Existing studies have shown that, for soils with different initial compaction

states, the mechanism of strength change of the specimens after suffusion is varied. With the loss of fine particles, specimen in the dense state often shows the disappearance of the peak strength after suffusion, while the initial loose sample reveals a reduction trend of the residual strength (Chen et al. 2016; Ke and Takahashi 2015; Rousseau et al. 2020).

Despite the suffusion phenomena having been widely investigated in the past decades, there are few comparative studies on the suffusion progression and strength property variation characteristics of gap-graded cohesionless soil with different particle-size distributions. In addition, under the stress release path, such as the strength evolution characteristics during the excavation of tunnels and foundation pits in the soil structure affected by suffusion need to be further explored. This paper intends to investigate the suffusion process and strength reduction characteristics of the post-suffusion cohesionless soil with the newly developed apparatus. The main objectives of this study are (1) to reproduce the suffusion process under a triaxial stress state; (2) to investigate the effect of the particle-size distribution (PSD) on fine particle erosion characteristics during the suffusion process; (3) to explore the strength reduction trend of soil specimens under different suffusion destruction level.

Laboratory experiments

Apparatus

A schematic diagram of the erosion–seepage–stress coupling test apparatus is shown in Fig. 1. The newly developed apparatus is designed based on a triaxial tester (Liang et al. 2017c, 2019). The main function of this apparatus is reproducing the internal erosion under an upward seepage and a triaxial stress condition. The apparatus is mainly composed of four components, including an upstream water supply system, a loading system, a soil–water separating system, and a water collecting system. The upstream water supply system is composed of an elevation-adjustable water tank and a water pipe. The height of the water tank can be adjusted by a fixed pulley, providing different hydraulic head required in the test. In addition, a plastic tube is connected to the air exchange hole at the top of the specimen. The tube ensures that the atmospheric pressure inside and outside the cap is balanced, which means that the downstream head on the specimen can remain stable throughout the test. Therefore, when the upstream water head is constantly in the process of suffusion, the hydraulic gradient applied to the specimen is also a stable value.

The loading system includes a confining stress loading system and a vertical stress loading system. During the test, confining stress is implemented by inflating pressurized gas into a Mariotte's bottle. Besides, the volumetric deformation

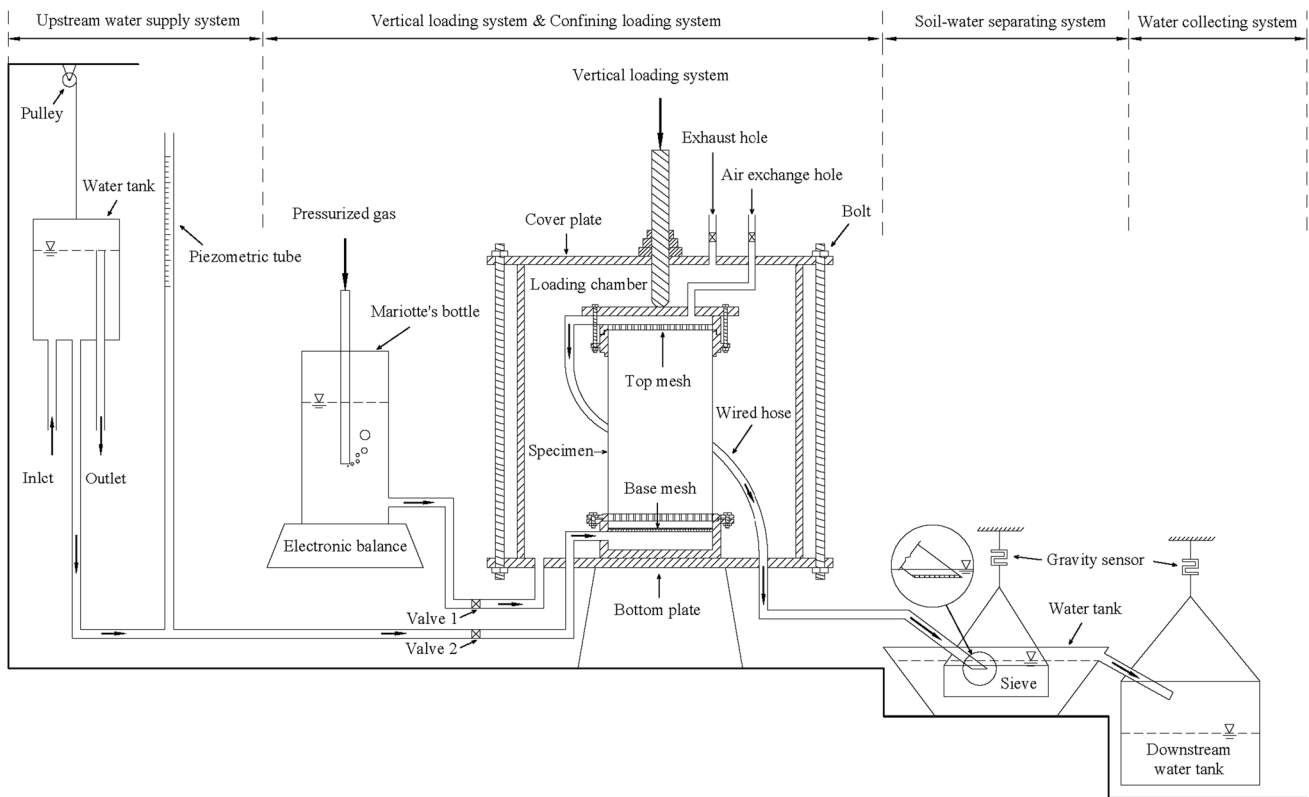


Fig. 1 Sketch map of the testing apparatus

of the specimen is monitored by the weight change of the Mariotte’s bottle. The vertical loading system with a vertical loading rod is arranged on top of the sample, and the vertical stress is applied by adjusting the pressure of the air pressure cylinder connected to the piston rod. Both confining pressure and vertical stress are measured by pressure transducers of each independent loading system. Under this triaxial stress state, the minor principal σ_3 and the intermediate principal stress σ_2 are equal to the confining pressure. The vertical stress applied by the vertical loading system is equivalent to the deviatoric stress, and the load applied by the vertical loading system is calculated as follows (Liang et al. 2017c):

$$F = \frac{pA}{1 - \sin \varphi} + pA', \tag{1}$$

where F is the load applied by the vertical loading system; p is the confining pressure; A is the cross-sectional area of the specimen column; A' is the cross-sectional area of the piston rod transferring the vertical load; φ is the friction angle of the tested soil; K_0 is the static lateral pressure coefficient.

The confining chamber is mainly composed of an external sealing device and a specimen sealing device. The height and the diameter of the specimen in the rubber film are 200 mm and 100 mm, respectively. Two meshes are allocated on the

bottom between the base and the specimen. The base mesh is placed at the bottom of the specimens to provide uniform seepage flow into the sample during the experiment. The diameter of the holes in the base mesh is 5.0 mm, and the spacing between the centers of the holes is 6.0 mm. A wire mesh with an aperture of 0.075 mm is adopted between the base mesh and the specimen to prevent fine particles from falling into the base pedestal. In addition, a steel top mesh with the same hole size as the base mesh is placed on top of the specimen. The top mesh functions as a loading plate, transmitting the vertical load on the top of the specimen evenly. The thickness of the top mesh is 2.5 mm, and the opening holes ensure that the fine particles eroded in the suffusion can flow out smoothly. (Liang et al. 2019).

The soil-carrying water flows out during the suffusion process, overflows from the top of the specimen, and then flows into the soil–water separating system through the wired hose. The height of the upper outlet pipe is almost flush with the top of the specimen, which ensures a smooth outflow of fine particles. A buffer net is set at the outlet position of the water pipe, and the outlet is submerged in water to mitigate the disturbance of the flow to the sensor. The eroded fine particles are gathered in the sieve in the soil–water separation system. The accumulative mass of fine particles is monitored by a gravity sensor combined with the

floating weight parameter of the fine particles. Subsequently, the overflowing water flow in the soil–water separating system flows into the water collection system, and the water flux during the suffusion process is measured by the weight of the water collected in real time. In the experiment, the acquisition frequency of the gravity sensor is 10 Hz. In the previous studies, the device has been used to investigate the suffusion process of cohesionless soils under isotropic and anisotropic stress environments successfully, and high critical hydraulic gradients (HCHG) and low critical hydraulic gradients (LCHG) are defined (Liang et al. 2017a, 2019; b).

Materials and specimen preparation

The soil used in the experiment is collected from the river beach formed by natural deposition on the banks of the upper reaches of the Yangtze River. First, the collected soil specimens are washed with tap water to eliminate impurities attached to the surface of soil particles. The particles with diameters ranging from 0.075 to 10.00 mm are selected with the sieving method (ASTM-D6913/D6913M-17 2017). For research purposes, particles with sizes between 0.25 and 1 mm were removed to reproduce the suffusion process in gap-graded cohesionless soils. Then, dividing the selected particles into five groups according to particle sizes of 0.075–0.25 mm, 1–2 mm, 2–5 mm, 5–8 mm, and 8–10 mm (Fig. 2a). The group ranging from 0.075 to 0.25 mm is

regarded as the finer particles (FP), and the rest of the four groups ranging from 1 to 10 mm are the coarser particles.

In this test, five groups of soil particles with different diameters are mixed fully to prepare three kinds of gap-graded specimens with varying ratios of the finer particles (FP). The three materials with different particle-size distributions are labeled as A, B, and C, respectively. Correspondingly, the coarse particles in three groups are named GA, GB, and GC (Fig. 2b). The finer particles (FP) accounted for 20%, 15%, and 20% of the total weight of A, B, and C, respectively. The basic characteristic parameters of these three materials are shown in Table 1. The specimens are prepared with the tamping method (ASTM-D7181-20 2020), and the moisture content is equal to 4.0%, close to the optimum moisture content (Andrianatrehina et al. 2015; Da-lang et al. 2020; Liang et al. 2017a). Each specimen is divided into ten parts by weight equally. The sample was then compacted to the target density in ten layers in a rubber film-wrapped chamber. The total weight of all specimens in the test is controlled at around 2906 g, and the dry density of the compacted specimens is around 1.85 g/cm³.

Experiment procedure

The experiment procedure in this study mainly consists of four steps, and the details of each test procedure are presented as follows.

Fig. 2 Materials used in this study: **a** photographs of the soil specimens and **b** grading curves of the soil particles

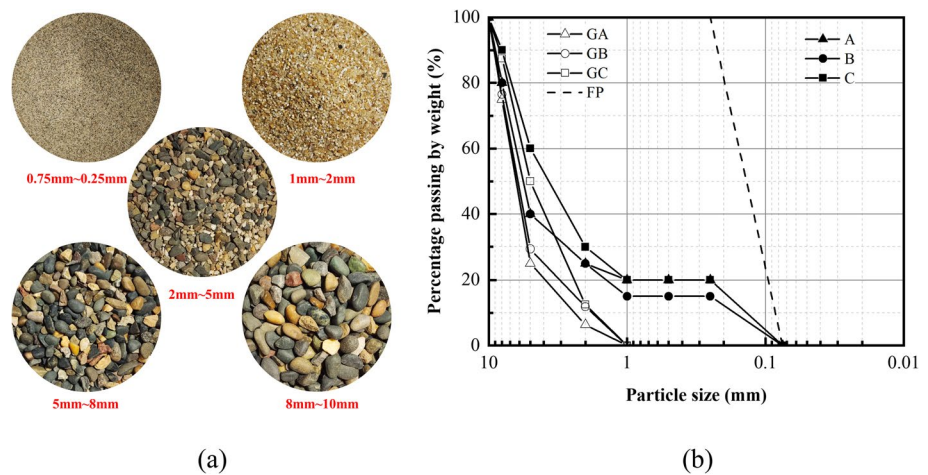


Table 1 Physical properties of soils specimens

No.	C_u	C_c	FP (%)	d_{10} (mm)	d_{30} (mm)	d_{60} (mm)	K_s (cm/s)	φ (°)
A	40.00	8.52	20	0.16	0.21	6.50	0.07	30.42
B	33.91	7.22	15	0.19	0.25	6.50	0.10	35.91
C	30.77	4.92	20	0.16	0.21	5.00	0.05	31.77

C_u is the coefficient of uniformity; C_c is the coefficient of curvature; FP is fine particle content; d_{10} is the diameter of the 10% mass passing in the coarse component; d_{30} is the diameter of the 30% mass passing in the coarse component, d_{60} is the diameter of the 60% mass passing in the coarse component; K_s is the initial saturated permeability coefficient; φ is the average friction angle of the unconsolidated soil

First, the stress is loaded to prevent the segregation of the soil (Suzuki et al. 2019). The confining stress is applied to the specimen prior to the vertical stress with a loading rate of 1 kPa/min recommended by the standard procedure (ASTM-D7181-20 2020; Chang and Zhang 2011). The application of the confining pressure is realized by adjusting the pressure air valve connected to the Mariotte's bottle. In this process, the pressure will be transmitted through the pressurized water to the rubber film in the pressure chamber, which will apply to the surface of the sample consequently. Then keeping the confining pressure constant, the vertical stress is applied to the top of the specimen by the vertical stress loading system.

The second step is to saturate the specimen. This operation is conducted by adjusting the height of the water tank in the upstream water supply system. After completing the loading and sealing procedures, slowly raise the water tank of the upstream water supply system until the water level gradually rises from the bottom of the specimen to the top. During this process, the ascending speed of the water tank is kept below 2 mm/min to prevent seepage deformation and fine particle migration of specimens. Afterward, the specimen is kept static for no less than 4.0 h to eliminate the air in the specimen. This process refers to the saturation procedure of the Standard for Soil Test Method (GB/T50123-1999) of China, which has been proved effective in the previous studies (Liang et al. 2017a, b, 2019).

The third step is to initiate the suffusion process by lifting the water tank in the upstream water supply system. Gradually increase the hydraulic head applied to the specimens at a rate of about 2 mm/min to trigger the suffusion. The critical hydraulic adopted in this experiment is larger than the high critical hydraulic gradient (HCHG) corresponding to the global loss of fine particles proposed by Liang et al. (2017a, b). That is, the hydraulic gradient is larger enough to wash the fine particles out. The drag force of the water flow in this critical hydraulic gradient state far exceeds the force required by the fine particles in the limit equilibrium state. In this process, the water flux and seepage velocity are calculated based on the change in the weight of the water collection system per unit of time. The mass of eroded fine particles is captured by the gravity sensor in the soil–water

separating system. In addition, the volume change of the specimen in the suffusion process is obtained by monitoring the weight of the Mariotte's bottle. An increase in the volume of water in the Mariotte's bottle is defined as positive, and conversely, a decrease in water volume is defined as negative. During the suffusion process, the mass of eroded fine particles to the total mass of the fine particles in the initial condition before suffusion is defined as an erosion ratio (ER).

The last step is to perform a shear strength test of the eroded specimen. When the cumulative mass of the eroded fine particles reaches the different ER in Table 2, the suffusion process is terminated by slowly reducing the hydraulic gradient. Then, gradually reduce the confining pressure and maintain the applied axial stress constant until the collapse of specimens. Specimen drainage is permitted during the shear process. The confining and vertical stress is monitored continuously until the failure of the specimen.

Experiment scenarios

In this experiment, a total number of 36 groups of suffusion tests are conducted using materials with different particle-size distributions (PSD), and the corresponding ER is listed in Table 2. It is particularly pointed out that A-1, B-1, and C-1 are reference experiments without particle loss. In these tests, to reproduce the actual stress environment of suffusion, the initial confining pressure and axial pressure applied during the suffusion process are determined according to Eq. (1) (Liang et al. 2017a, b, 2019)

$$\sigma_3 = \sigma_1 K_0 = \sigma_1 (1 - \sin \varphi), \tag{2}$$

where σ_1 and σ_3 are the major principal stress and the minor principal stress; respectively; K_0 is the static lateral pressure coefficient; φ is the average friction angle of the unconsolidated soil. According to triaxial shear tests, the average friction angle of the soil consisting of the three PSDs under a similar dry density is about 32.7°. Therefore, the static lateral pressure coefficient is uniformly taken as 0.46 based on Eq. (2). The minor principal stress and the major principal stress adopted in the test are 25 kPa and 54.4 kPa,

Table 2 Erosion ratio of fine particles in different test groups

No.	ER (%)	No.	ER (%)	No.	ER (%)	No.	ER (%)	No.	ER (%)	No.	ER (%)
A-1	0.0	A-7	14.6	B-1	0.0	B-7	15.1	C-1	0.0	C-7	15.0
A-2	4.7	A-8	17.0	B-2	5.7	B-8	16.4	C-2	5.7	C-8	17.0
A-3	6.8	A-9	21.8	B-3	7.6	B-9	18.3	C-3	6.6	C-9	19.0
A-4	8.5	A-10	24.6	B-4	8.2	B-10	19.5	C-4	8.0	C-10	20.3
A-5	9.9	A-11	30.8	B-5	9.5	B-11	20.2	C-5	9.0	C-11	25.6
A-6	10.4	A-12	35.0	B-6	11.3	B-12	25.0	C-6	11.3	C-12	30.0

ER = fine particles' erosion ratio

respectively. The mean effective stress for consolidation considered in this experiment is 51.46 kPa. This condition corresponds to the vertical effective stress at a depth of 5 m when the groundwater table is at the ground surface and the soil ground is fully saturated, which is widely present along the Yangtze River (Ke and Takahashi 2015).

Results

Hydraulic characteristics in the process of suffusion

Figure 3 depicts the typical relations between the seepage velocity, v , and the hydraulic gradient, i . Throughout the experiments, the $v \sim i$ curves with different groups of materials show a similar development trend. In the initial stage, the hydraulic gradient slowly increases as the upstream water tank rises. The seepage velocity increases in an approximately linear trend with the increase of i , which conforms to the characteristics of Darcy's law. According to Darcy's law, the average hydraulic conductivities of the specimens for experiments A-12, B-12, and C-12 are 0.17 cm/s, 0.23 cm/s, and 0.10 cm/s, respectively. The critical hydraulic gradients of the three materials obtained from the experiments are 0.770, 0.665, and 0.895, respectively. However, the relationship between the hydraulic gradient and seepage velocity no longer follows Darcy's law after the hydraulic gradient reaches a critical value. Under a constant critical hydraulic gradient, the seepage velocity increases rapidly and tends to a constant level (Skempton and Brogan 1994). When the hydraulic gradient reaches a critical value, fine particles start to be carried out by the water flow. The mass of the finer particles collected by the sieve of the soil–water separating system increase continually. This phenomenon could be

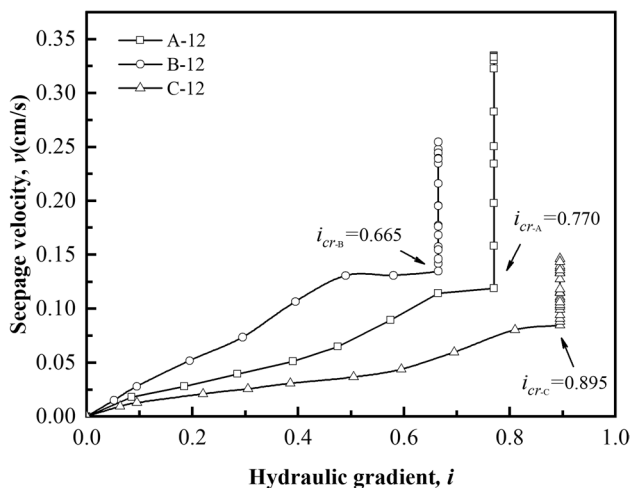


Fig. 3 Response of seepage velocity with the incremental hydraulic gradient

regarded as a sign of the initiation of the suffusion. To further explore the suffusion process, the stage before reaching the critical hydraulic gradient is defined as the steady seepage stage, i.e., stage 1 (S1). In this experiment, the duration of this period lasted approximately 70 min.

During the tests, as the water head applied to the specimen increases, the weight data collected by the downstream water collection system increases gradually. The water fluxes in the above-mentioned experiment groups are plotted as a function of the time in Fig. 4. This figure reveals that the water fluxes maintain a similar growth rate over time in the S1 stage. After reaching the critical hydraulic gradient, the preferential flow paths inside the specimen gradually expanded with the loss of fine particles. During this process, under the condition of constant head, the water flux gradually increases at a rate lower than that of the S1 stage and tends to a constant value. About 110 min after the hydraulic gradient reached the critical value, that is, after the whole experiment is carried out for 180 min, the scale of the preferential seepage paths in the specimen stabilized gradually. The water flux presents varying growth trends and gradually stabilizes in the end. Ultimate, the water fluxes of the three test specimens, A-12, B-12, and C-12, finally stabilized at 26.19 cm³/s, 19.10 cm³/s, and 9.65 cm³/s, respectively.

Based on the above characteristics, the process from reaching the critical hydraulic gradient until the stable seepage channel is formed is defined as the suffusion initiation stage (S2). Next, the process in which the seepage flux remains substantially constant is defined as the suffusion equilibrium stage (S3). In the S3 stage, along with the continuous loss of fine particles, the scale of the preferential seepage paths no longer expands. This is attributed to the water head being constant throughout the process, and the hydraulic gradient in the S3 stage is already lower than the

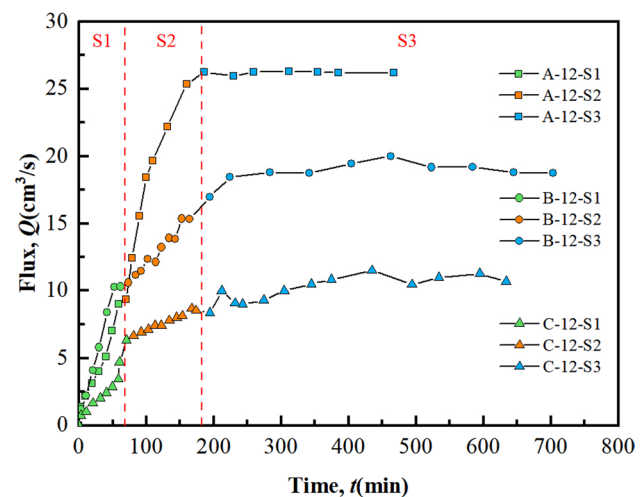


Fig. 4 Variation of the flux in the suffusion process

value for further continuous expansion of the post-suffusion specimen. In addition, the effect of external stress will also limit the continuous expansion of the suffusion and will promote the suffusion process to a new equilibrium state.

Erosion process and volumetric strain characteristics

During the suffusion process, finer particles are washed out continuously when the hydraulic gradient increases to the critical value. The moment when the hydraulic gradient reaches the critical value is determined as the beginning of the erosion. As shown in Fig. 5, the accumulative mass of the eroded fine particles increased approximately following a linear relationship with the increment of erosion time. The mass of fine particle loss per minute is defined as the fine particle loss rate (LR). It reveals that the LR of each group is roughly a constant value during the S2 stage, and the average LR of the A-12, B-12, and C-12 groups are 0.97 g/min, 0.39 g/min, and 0.43 g/min, respectively. In the S3 stage, the average LR of the A-12, B-12, and C-12 test groups dropped to 0.29 g/min, 0.12 g/min, and 0.32 g/min, with a gap of 0.68 g/min, 0.27 g/min, and 0.11 g/min, respectively. With the development of suffusion, the average LR in the S3 stage is lower than in the S2 stage. As for the entire suffusion process, the average LR of the A-12, B-12, and C-12 test groups is 0.48 g/min, 0.17 g/min, and 0.35 g/min, respectively. The erosion process of the B-12 group with relatively low fine particle content is the slowest.

The volumetric deformation of the specimen is monitored by weighting the Mariotte’s bottle. It should be noted that the volume change value monitored is all negative; that is, the specimen exhibited a contraction trend with the progress of suffusion. In this study, the absolute value is taken for analysis, and the evolution of volumetric strain with erosion

time is shown in Fig. 6. It reveals that the maximum volumetric strain of the A-12, B-12, and C-12 test groups are 0.52%, 0.75%, and 0.57%, respectively. Specifically, the volumetric strain of the C-12 group reveals a linear relationship with erosion time, and its growth rate is almost constant throughout the suffusion process, similar to its erosion characteristics of fine particles. However, for the A-12 and B-12 groups, the volumetric strain growth rate in the S2 stage is significantly higher than in the S3 stage. Specifically, from the S2 to S3 stages, the average growth rate of volumetric strain decreased from 0.00296% per minute to 0.00058% per minute in groups A-12. Similarly, in the B-12 group, the mean growth rate of volumetric strain decreased from 0.00333% per minute to 0.00073% per minute.

Strength reduction of post-suffusion specimen

After the suffusion experiments, shear strength tests are conducted to measure the strength of the post-suffusion soil specimens. In this study, failure is defined as the soil state in which the principal stress ratio ($R, R = \sigma_1/\sigma_3$) obtained at an axial strain of 15% (Ke and Takahashi 2015); and correspondingly, the soil strength refers to the principal stress ratio at an axial strain of 15%. The principal stress ratio at the failure state is listed in Table 3. The relation curves of axial strain and principal stress ratio of the no-eroded specimens (A-1, B-1, C-1) and part of the eroded specimens (A-12, B-12, C-12) are plotted in Fig. 7. The no-eroded specimens show a slight strain-softening responses. In addition, as for uneroded specimens, the peak shear strength of B-1 with a fine particle content of 15% reveals the lowest. The strain-softening phenomenon in the C-1 and A-1 groups is more significant than in the B-1 group. However, the eroded soil behaves like loose

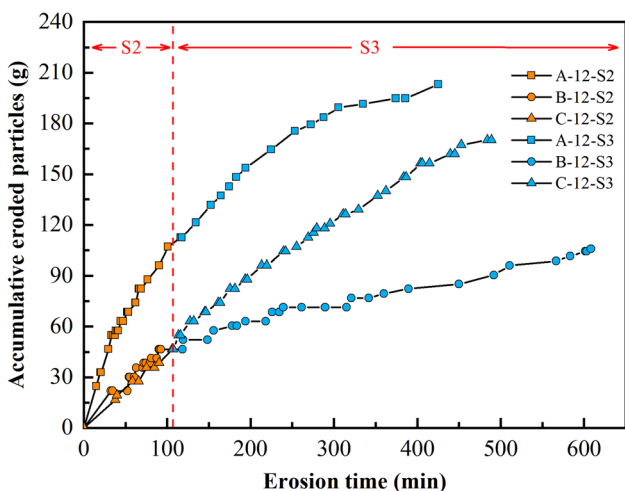


Fig. 5 Accumulative fine particles loss within the suffusion test period

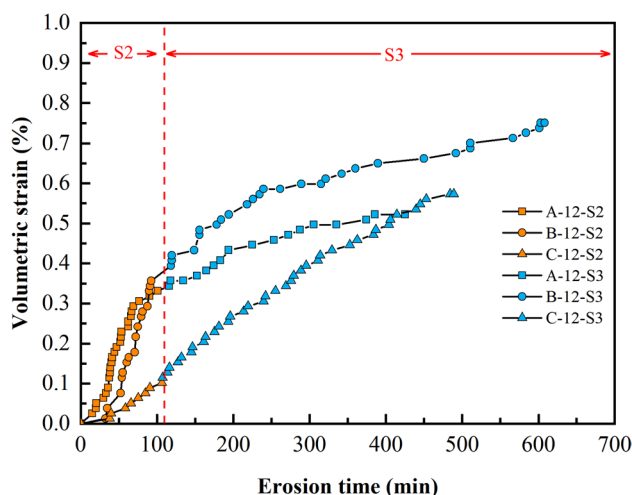


Fig. 6 Volumetric strain within the suffusion test period

Table 3 The principal stress ratio of the specimen at shear failure

No.	R_f	No.	R_f	No.	R_f	No.	R_f	No.	R_f	No.	R_f
A-1	5.54	A-7	3.91	B-1	5.14	B-7	4.88	C-1	5.45	C-7	4.49
A-2	5.32	A-8	3.83	B-2	5.03	B-8	4.86	C-2	5.14	C-8	4.34
A-3	5.17	A-9	3.63	B-3	5.00	B-9	4.82	C-3	5.03	C-9	4.23
A-4	5.08	A-10	3.37	B-4	4.99	B-10	4.71	C-4	4.87	C-10	4.09
A-5	4.27	A-11	3.30	B-5	4.97	B-11	4.63	C-5	4.68	C-11	4.03
A-6	4.13	A-12	3.24	B-6	4.93	B-12	4.54	C-6	4.54	C-12	3.94

R_f is the principal stress ratio at shear failure

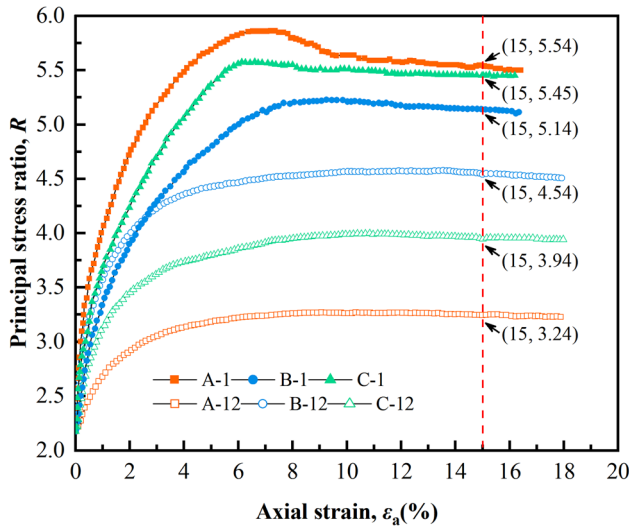


Fig. 7 Relationship between principal stress ratio and axial strain

soil, and the peak strength disappears, showing a trend that flattened out at large strains after substantial compression (Andersen and Schjetne 2013; Mao et al. 2021; Rousseau et al. 2020). This is attributed to the continued erosion of fine particles leading to an increase in the void ratio and considerably loosening the soil structure (Mao et al. 2021; Suzuki et al. 2019; Chang and Zhang 2011).

To further explore the strength reduction of the post-suffusion cohesionless soil, the strength reduction factor ΔR is defined as follows (Ke and Takahashi 2012):

$$\Delta R = 1 - \frac{\tan \varphi_f}{\tan \varphi_0} \tag{3}$$

where ΔR is the strength reduction by percentage after erosion; φ_f is the friction angle of shear failure after suffusion; φ_0 is the friction angle of shear failure before suffusion. φ_0 corresponds to the test group of A-1, B-1, and C-1. According to the above formula, it can be found that the value of ΔR is between 0 and 1, and the closer it is to 1, the greater the strength reduction degree. In a triaxial compression test,

friction angles φ are defined as (Sadrekarimi and Olson 2011)

$$\varphi = \sin^{-1} \left(\frac{3\eta}{6 + \eta} \right), \tag{4}$$

where η is the axisymmetric principal stress ratio $[=3(\sigma_1 - \sigma_3)/(\sigma_1 + 2\sigma_3)]$; σ_1 and σ_3 are the major principal stress and minor principal stress.

Utilizing Eqs. (3) and (4), combined with the principal stress ratio at the failure in Table 3, the friction angle of post-suffusion soil specimens is calculated, as shown in Fig. 8a. Correspondingly, the relationship between the strength reduction factor and the ER is plotted in Fig. 8b. From the figures, it can be found that with the increase of ER, the strength of the soil shows a decreasing trend overall, which is similar to the experiment results of Mehdizadeh et al. (2017). Furthermore, when the ER is less than 6%, the strength reduction factors are all less than 0.05. That is, the loss of a small number of fine particles has little influence on the strength properties. With the development of suffusion, the strength reduction of the soil from group A and group C is much more significant than in group B, when the ER is nearly 10%. It's slightly higher than the 4% in Chang's research (Chang and Zhang 2013). When the ER reaches the maximum value in Table 2, the friction angles of the specimen in groups A, B, and C are reduced by 12.04°, 2.67°, and 7.12°, respectively. The maximum strength reduction factors of A, B, and C reach 0.35, 0.09, and 0.22. The strength reduction phenomenon for the test groups A and C with relatively higher fine particle content is much more significant, with a maximum decrease ratio of 27.39% and 16.31%, respectively. The diversity of evolution trends for strength reduction is attributed to the difference in the skeleton of the three different graded soils, which will be analyzed further in the following section.

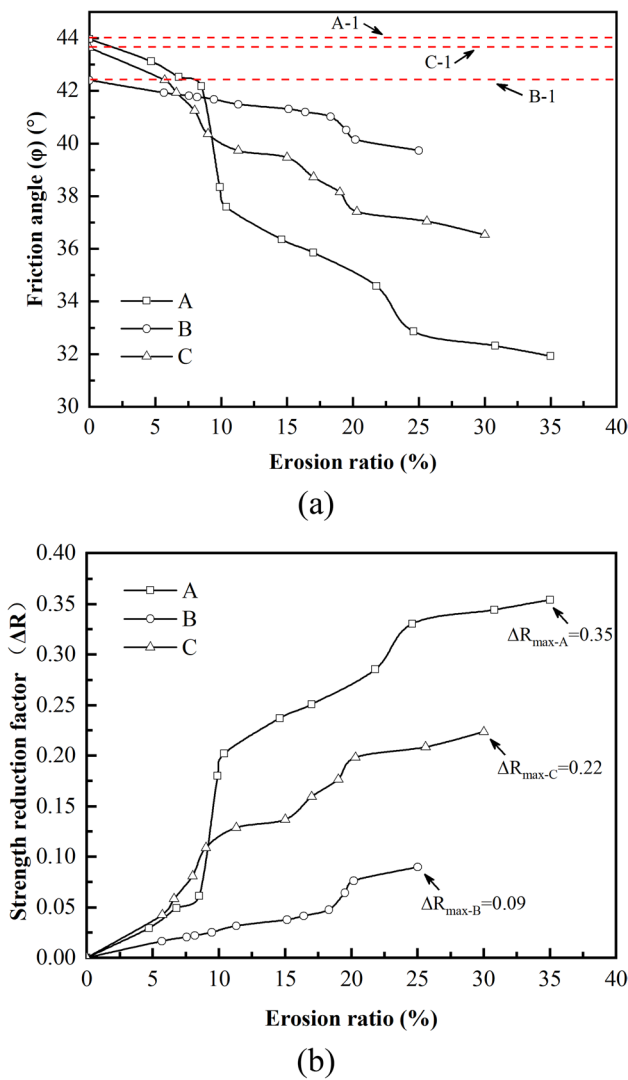


Figure 8 Strength property variation: **a** friction angle with different erosion ratio; **b** the relationship between strength reduction factor and erosion ratio

Analysis and discussion

Internal stability assessment and fine particle migration characteristics

Internal stability represents the ability of coarse particles in soil to prevent the loss of fine particles, which also performs as an important indicator for assessing the probability of fine particle migration in the suffusion process (Chang and Zhang 2013). Generally, the internal stability of a gap-graded cohesionless soil is influenced by geometric conditions, hydraulic conditions, and mechanical conditions (Chang and Zhang 2013; Marot et al. 2015). As a significant geometric factor to describe the characteristics of soil, the effects of the PSD on the internal stability of cohesionless

Table 4 Geometrical and mechanical properties of specimens with different PSDs

PSD	P (%)	$(H/F)_{\min}$	G_r	D_{15}/d_{85}
A	20	0	4	6.5
B	15	0	4	5.3
C	20	0	4	4.8

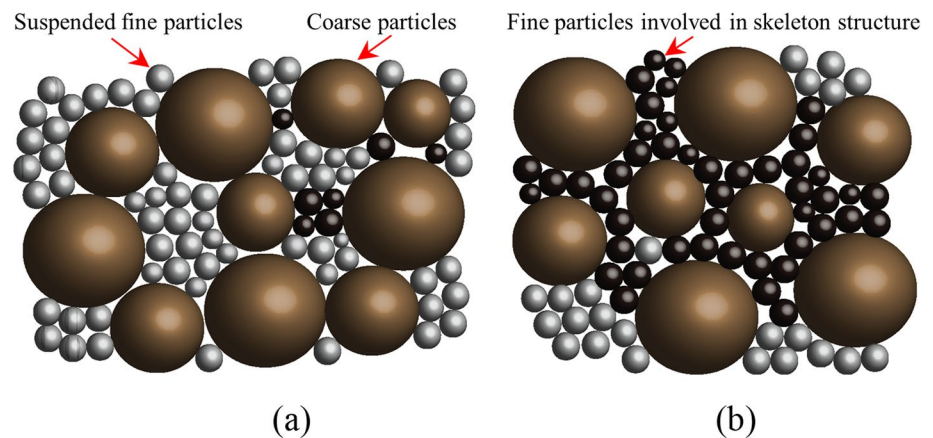
P is the fine particle content; H is the weight fraction of the soil in size ranging from d to $4d$; F is the weight fraction of the soil finer than size d ; G_r is the gap ratio; D_{15} is the diameter of the 15% mass passing in the coarse component; d_{85} is the diameter of the 85% mass passing in the fine component

soil have been widely explored, and various criteria have been proposed by statistical methods. One of the most currently used criteria is the ratio $(H/F)_{\min}$ proposed by Kenney and Lau (1985) and Skempton and Brogan (1994). They suggested that the soil is internally unstable when $(H/F)_{\min} < 1$ (Kenney and Lau 1985). Liu proposed to adopt the finer fraction P (%) to assess the instability and suggested that the soil is internally unstable when $P < 25$ (Liang et al. 2017b). In addition, Zhang et al. proposed a criterion for judging internal stability by combining fine particle content and the gap ratio (Chang and Zhang 2013; Kodieh et al. 2021). On the other hand, a simple method of assessing internal stability was put forward by Kezdi, following the concept of Terzaghi's filter rule (Ke and Takahashi 2014). According to the above-mentioned particle-size distribution-based criteria and the properties listed in Table 4, the soils adopted in this study are all potentially unstable. While the criteria in Table 4 are satisfactory in assessing the internal stability of the gap-graded cohesionless soils, their performance requires further evaluation when the material with great similarity to PSD. Since the $(H/F)_{\min}$ and G_r in this research cannot reflect the difference of materials with different PSD, to further evaluate the fine particle migration characteristics, the magnitude of the D_{15}/d_{85} is adapted to assess the loss potential of fine particles (Sherard et al. 1984). According to the evolution characteristics of the suffusion process, for specimens with the same fine particle content, the larger the D_{15}/d_{85} , the lower the critical hydraulic gradient required to trigger the suffusion, and the faster the fine particle loss rate, that is, the easier the migration of the fine particles. However, the feasibility of evaluating the migration potential of fine particles based on the Kezdi criterion needs further study (Benamar et al. 2019).

The influence of soil skeleton structure on strength reduction

Figure 9a, b depicts two different types of soil skeleton structures. Existing research reveals that the migration and rearrangement of fine particles will significantly impact

Fig. 9 Schematic diagram of different soil skeleton structures: **a** coarse particles and coarse particles are in contact with each other, and **b** coarse particles and fine particles are in contact with each other



the specimen's microstructure (Da-lang et al. 2020; Ke and Takahashi 2014; Liang et al. 2017b). This process will inevitably lead to changes in the mechanical properties of the soil (Lee et al. 2021). Along with the loss of fine particles, the strength property of the specimens with different soil skeleton structures reveals different trends of decreasing characteristics. Under a similar ER, the strength of the group B soil specimens with the lowest content of initial fine particles shows the smallest strength reduction change. This is attributed to the fact that most of the soil skeletal structures of the samples in group B are formed in such a mode that the coarse particles are in contact with each other, as shown in Fig. 9a. In this case, part of the fine particles is not involved in the force transmission framework structure but filled in the pores between the coarse particles in a 'suspended' state (Da-lang et al. 2020). Therefore, the loss of the fine particles not yet involved in the force-transfer framework of the soil structure has little influence on the strength of the soil specimens (Dassanayake et al. 2022; Mao et al. 2021).

However, when the content of fine particles exceeds the pores of coarse particles and is greater than the critical value in the fully filled state, part of the fine particles participates in the force-transfer framework of the soil skeleton structure, as shown in Fig. 9b (Da-lang et al. 2020; Liang et al. 2017b). In this circumstance, the loss of fine particles will cause a rearrangement of the skeleton, significantly impacting the skeleton structure of specimens (Ke and Takahashi 2014). This mechanism will result in a decrease in the strength of the post-suffusion specimens (Mao et al. 2021). Just like the group A and group C in the experiment.

Conclusions

In this study, a set of erosion–seepage–stress coupling test apparatus is used to carry out the suffusion test under triaxial stress environments with three kinds of gap-graded cohesionless soil, and the following conclusions are drawn.

The critical hydraulic gradient of gap-graded cohesionless soil suffusion is related to the relative content of fine and coarse particles. When the fine particle content is the same, the filter criteria D_{15}/d_{85} can be used to judge the difficulty of fine particle migration and the magnitude of the critical hydraulic gradient. The evolution process of suffusion is divided into three typical stages based on the hydraulic characteristics and fine particle loss trend: the steady seepage stage (S1), the suffusion initiation stage (S2), and the suffusion equilibrium stage (S3).

Under the same triaxial stress environment, specimens with a relatively low content of fine particles group show the slowest erosion process. The influence of suffusion on the strength characteristics of cohesionless soil is affected by the combined effects of particle-size distribution and the degree of erosion. When the ER is greater than 6%, the strength of the three kinds of gap-graded cohesionless soil decreases significantly with the increase of ER. However, suffusion has less effect on the strength of the cohesionless soil with a lower fine particle content, i.e., corresponding to 15% of the fine particle content in this study, which is attributed to the difference in soil skeleton structure.

This study only explored the suffusion process of gap-graded cohesionless soil in a stable stress environment and the strength changes characteristics of the soil specimen after suffusion. However, the stress path in engineering is much more complex, and the types of soil specimens are abundant and diverse. The follow-up needs to conduct in-depth research on the seepage–erosion–stress coupling process of different cohesionless soils in complex stress environments.

Acknowledgements This work is supported by the National Key Research and Development Program of China (Grant nos. 2019YFC1510802 and 2018YFC1504700), the National Natural Science Foundation of China (Grant no. 41530640), the National Natural Science Foundation of Chongqing, China (Grant no. cstc2018jcyjAX0559), and the Scientific Research and Innovation Program for Graduate Students of Chongqing (Grant no. CYB22234).

Author contributions YL: conceptualization, methodology, investigation, and funding acquisition. BZ: writing—original draft, and data analysis. YY: investigation, resources. HZ: visualization. LD: data curation.

Availability of data and materials Some or all data generated during the study are available from the corresponding author by request.

Declarations

Conflict of interest The authors declare that they have no known competing financial interests or personal relationships that could have appeared to influence the work reported in this paper.

References

- Andersen KH, Schjetne K (2013) Database of friction angles of sand and consolidation characteristics of sand, silt, and clay. *J Geotech Geoenviron Eng* 139:1140–1155. [https://doi.org/10.1061/\(asce\)gt.1943-5606.0000839](https://doi.org/10.1061/(asce)gt.1943-5606.0000839)
- Andrianatrehina L, Souli H, Rech J, Taibi S, Fry J-J, Ding L, Fleureau J-M (2015) Analysis of the internal stability of coarse granular materials according to various criteria. *Eur J Environ Civ Eng* 20:936–953. <https://doi.org/10.1080/19648189.2015.1084385>
- ASTM-D6913/D6913M-17 (2017M) Standard test methods for particle-size distribution (gradation) of soils using sieve analysis. ASTM International, West Conshohocken
- ASTM-D7181-20 (2020) Standard test method for consolidated drained triaxial compression test for soils. ASTM International, West Conshohocken
- Benamar A, Correia dos Santos RN, Bennabi A, Karoui T (2019) Suffusion evaluation of coarse-graded soils from Rhine dikes. *Acta Geotech* 14:815–823. <https://doi.org/10.1007/s11440-019-00782-1>
- Bonelli SE (2012) *Erosion of geomaterials*. Wiley, New York
- Chang D, Zhang LM (2011) A stress-controlled erosion apparatus for studying internal erosion in soils. *Geotech Test J* 34:11. <https://doi.org/10.1520/gtj103889>
- Chang DS, Zhang LM (2013) Extended internal stability criteria for soils under seepage. *Soils Found* 53:569–583. <https://doi.org/10.1016/j.sandf.2013.06.008>
- Chen C, Zhang LM, Chang DS (2016) Stress-strain behavior of granular soils subjected to internal erosion. *J Geotech Geoenviron Eng*. [https://doi.org/10.1061/\(asce\)gt.1943-5606.0001561](https://doi.org/10.1061/(asce)gt.1943-5606.0001561)
- Chen L, He J-j, Yao B-b, Lei C-w, Zhang Z (2019) Influence of the initial relative density on the drained strength properties of soils subjected to internal erosion. *Soil Mech Found Eng* 56:273–279. <https://doi.org/10.1007/s11204-019-09602-w>
- Chen L, Wan Y, He J-J, Luo C-M, Yan S-F, He X-F (2021a) Experimental study on the suffusion mechanism of gap-graded soils under an exceedance hydraulic gradient. *Nat Hazards* 109:405–439. <https://doi.org/10.1007/s11069-021-04842-2>
- Chen R, Liu L, Li Z, Deng G, Zhang Y, Zhang Y (2021b) A novel vertical stress-controlled apparatus for studying suffusion along horizontal seepage through soils. *Acta Geotech* 16:2217–2230. <https://doi.org/10.1007/s11440-021-01164-2>
- Da-lang T, Qiang X, Xiang F, Jianhua Z (2020) Experimental study on the effect of fine contents on internal erosion in natural soil deposits. *Bull Eng Geol Env* 79:4135–4150. <https://doi.org/10.1007/s10064-020-01829-4>
- Dassanayake SM, Mousa A, Ilankoon S, Fowmes GJ (2022) Internal instability in soils A critical review of the fundamentals and ramifications. *Transp Res Rec* 2676:26. <https://doi.org/10.1177/03611981211056908>
- Deng G, Cao K, Chen R, Zhang X, Yin Q, Zhou H (2018) A simple approach to evaluating leakage through thin impervious element of high embankment dams. *Environ Earth Sci*. <https://doi.org/10.1007/s12665-017-7195-3>
- Deng G, Zhang L-L, Chen R, Liu L-L, Shu K-X, Zhou Z-L (2020) Experimental investigation on suffusion characteristics of cohesionless soils along horizontal seepage flow under controlled vertical stress. *Front Sci*. <https://doi.org/10.3389/feart.2020.00195>
- Douglas KJ, Fell R, Peirson WL, Studholme H (2019) Experimental investigation of global backward erosion and suffusion of soils in embankment dams. *Can Geotech J* 56:789–807. <https://doi.org/10.1139/cgj-2018-0088>
- Horikoshi K, Takahashi A (2015) Suffusion-induced change in spatial distribution of fine fractions in embankment subjected to seepage flow. *Soils Found* 55:1293–1304. <https://doi.org/10.1016/j.sandf.2015.09.027>
- Hu Z, Yang ZX, Zhang YD (2020a) CFD-DEM modeling of suffusion effect on undrained behavior of internally unstable soils. *Comput Geotech*. <https://doi.org/10.1016/j.compgeo.2020.103692>
- Hu Z, Zhang Y, Yang Z (2020b) Suffusion-induced evolution of mechanical and microstructural properties of gap-graded soils using CFD-DEM. *J Geotech Geoenviron Eng*. [https://doi.org/10.1061/\(asce\)gt.1943-5606.0002245](https://doi.org/10.1061/(asce)gt.1943-5606.0002245)
- Huang Z, Bai Y, Xu H, Sun J (2020) A theoretical model to predict suffusion-induced particle movement in cohesionless soil under seepage flow. *Eur J Soil Sci* 72:1395–1409. <https://doi.org/10.1111/ejss.13062>
- Israr J, Aziz M (2019) Integrating the role of relative density on assessing internal stability of granular filters using existing geometrical methods. *Arab J Geosci*. <https://doi.org/10.1007/s12517-019-4850-x>
- Jiang F, Guan Z (2020) Analysis of the critical hydraulic condition of subterranean soil erosion and its factors. *Geotech Geol Eng* 38:6601–6609. <https://doi.org/10.1007/s10706-020-01457-5>
- Ke L, Takahashi A (2012) Strength reduction of cohesionless soil due to internal erosion induced by one-dimensional upward seepage flow. *Soils Found* 52:698–711. <https://doi.org/10.1016/j.sandf.2012.07.010>
- Ke L, Takahashi A (2014) Experimental investigations on suffusion characteristics and its mechanical consequences on saturated cohesionless soil. *Soils Found* 54:713–730. <https://doi.org/10.1016/j.sandf.2014.06.024>
- Ke L, Takahashi A (2015) Drained monotonic responses of suffusional cohesionless soils. *J Geotech Geoenviron Eng*. [https://doi.org/10.1061/\(ASCE\)GT.1943-5606.0001327](https://doi.org/10.1061/(ASCE)GT.1943-5606.0001327)
- Kenney TC, Lau D (1985) Internal stability of granular filters. *Can Geotech J* 22:11. <https://doi.org/10.1139/t85-029>
- Kodieh A, Gelet R, Marot D, Fino AZ (2021) A study of suffusion kinetics inspired from experimental data: comparison of three different approaches. *Acta Geotech* 16:19. <https://doi.org/10.1007/s11440-020-01016-5>
- Lee H-J, Kim I-H, Chung C-K (2021) Evaluation of the internal stability of well-graded silty sand through the long-term seepage test. *Int J Geo-Eng*. <https://doi.org/10.1186/s40703-021-00151-6>
- Li S, Russell AR, Wood DMJCGJ (2019) Influence of particle-size distribution homogeneity on shearing of soils subjected to internal erosion. *Can Geotech J*. <https://doi.org/10.1139/cgj-2019-0273>
- Li Z, Luo X, Bi J, Shen H (2020) Numerical modelling of internal erosion process in gravel soils based on the percolation analytical method. *Environ Earth Sci*. <https://doi.org/10.1007/s12665-020-09101-4>
- Liang Y, Yeh T-CJ, Wang J, Liu M, Zha Y, Hao Y (2017a) Onset of suffusion in upward seepage under isotropic and anisotropic stress

- conditions. *Eur J Environ Civ Eng* 23:1520–1534. <https://doi.org/10.1080/19648189.2017.1359110>
- Liang Y, Yeh T-CJ, Zha Y, Wang J, Liu M, Hao Y (2017b) Onset of suffusion in gap-graded soils under upward seepage. *Soils Found* 57:849–860. <https://doi.org/10.1016/j.sandf.2017.08.017>
- Liang Y, Zeng C, Wang JJ, Liu MW, Jim Yeh TC, Zha YY (2017c) Constant gradient erosion apparatus for appraisal of piping behavior in upward seepage flow. *Geotech Test J*. <https://doi.org/10.1520/gtj20150282>
- Liang Y, Yeh T-CJ, Chen Q, Xu W, Dang X, Hao Y (2019) Particle erosion in suffusion under isotropic and anisotropic stress states. *Soils Found* 59:1371–1384. <https://doi.org/10.1016/j.sandf.2019.06.009>
- Luo Y, Huang Y (2020) Effect of open-framework gravel on suffusion in sandy gravel alluvium. *Acta Geotech* 15:2649–2664. <https://doi.org/10.1007/s11440-020-00933-9>
- Luo Y, Luo B, Xiao M (2019) Effect of deviator stress on the initiation of suffusion. *Acta Geotech* 15:1607–1617. <https://doi.org/10.1007/s11440-019-00859-x>
- Ma Z, Wang Y, Ren N, Shi W (2018) A coupled CFD-DEM simulation of upward seepage flow in coarse sands. *Mar Georesour Geotechnol* 37:589–598. <https://doi.org/10.1080/1064119x.2018.1466223>
- Mao W, Xu C, Yang Y (2021) Investigation on strength degradation of sandy soil subjected to concentrated particle erosion. *Environ Earth Sci*. <https://doi.org/10.1007/s12665-021-10123-9>
- Marot D, Lev D, Garnier J, Thorel L, Audrain P (2012) Study of scale effect in an internal erosion mechanism centrifuge model and energy analysis. *Eur J Environ Civ Eng* 16:19. <https://doi.org/10.1080/19648189.2012.667203>
- Marot D, Rohim A, Nguyen NH, Bendahmane F, Sibille L (2015) Systematic methodology for characterization of suffusion sensibility. In: *Scour and erosion: Proceedings of the 7th international conference on scour and erosion*. CRC Press, Perth, Australia. p 213
- Masi M, Ferdos F, Losito G, Solari L (2020) Monitoring of internal erosion processes by time-lapse electrical resistivity tomography. *J Hydrol*. <https://doi.org/10.1016/j.jhydrol.2020.125340>
- Mehdizadeh A, Disfani MM, Evans R, Arulrajah A, Ong DEL (2017) Mechanical consequences of suffusion on undrained behaviour of a gap-graded cohesionless soil—an experimental approach. *Geotech Test J*. <https://doi.org/10.1520/gtj20160145>
- Perzmaier S (2007) *Hydraulic criteria for internal erosion in cohesionless soil*, 1st edn. CRC Press, Boca Raton
- Prasomsri J, Takahashi A (2020) The role of fines on internal instability and its impact on undrained mechanical response of gap-graded soils. *Soils Found* 60:1468–1488. <https://doi.org/10.1016/j.sandf.2020.09.008>
- Rochim A, Marot D, Sibille L, Le VT (2017) Effects of hydraulic loading history on suffusion susceptibility of cohesionless soils. *J Geotech Geoenviron Eng*. [https://doi.org/10.1061/\(ASCE\)GT.1943-5606.0001673](https://doi.org/10.1061/(ASCE)GT.1943-5606.0001673)
- Rousseau Q, Sciarra G, Gelet R, Marot D (2020) Modelling the pore- elastoplastic behaviour of soils subjected to internal erosion by suffusion. *Int J Numer Anal Methods Geomech* 44:20. <https://doi.org/10.1002/nag.3014>
- Sadrekarami A, Olson SM (2011) Critical state friction angle of sands. *Géotechnique* 61:771–783. <https://doi.org/10.1680/geot.9.P.090>
- Sherard JL, Dunnigan LP, Talbot JR (1984) Basic properties of sand and gravel filters. *J Geotech Eng* 110:684–700. [https://doi.org/10.1061/\(ASCE\)0733-9410\(1984\)110:6\(684\)](https://doi.org/10.1061/(ASCE)0733-9410(1984)110:6(684))
- Skempton AW, Brogan JM (1994) Experiments on piping in sandy gravels. *Geotechnique* 44:12. <https://doi.org/10.1680/geot.1994.44.3.449>
- Ślusarek J, Łupieżowicz M (2021) Analysis of damage to structures as a result of soil suffusion. *Eng Fail Anal*. <https://doi.org/10.1016/j.engfailanal.2020.105058>
- Suzuki Y, Carotenuto P, Dyvik R, Jostad HP (2019) Experimental study of modeling partially drained dense sand behavior in monotonic triaxial compression loading tests. *Geotech Test J* 43:17. <https://doi.org/10.1520/GTJ20190097>
- Xiong H, Yin Z-Y, Zhao J, Yang Y (2020) Investigating the effect of flow direction on suffusion and its impacts on gap-graded granular soils. *Acta Geotech* 16:399–419. <https://doi.org/10.1007/s11440-020-01012-9>
- Yang J, Yin Z-Y, Laouafa F, Hicher P-Y (2019) Modeling coupled erosion and filtration of fine particles in granular media. *Acta Geotech* 14:1615–1627. <https://doi.org/10.1007/s11440-019-00808-8>
- Zhou W, Ma Q, Ma G, Cao X, Cheng Y (2020a) Microscopic investigation of internal erosion in binary mixtures via the coupled LBM-DEM method. *Powder Technol* 376:31–41. <https://doi.org/10.1016/j.powtec.2020.07.099>
- Zhou Z, Li Z, Ranjith PG, Wen Z, Shi S, Wei C (2020b) Numerical simulation of the influence of seepage direction on suffusion in granular soils. *Arab J Geosci*. <https://doi.org/10.1007/s12517-020-05504-6>

Publisher's Note Springer Nature remains neutral with regard to jurisdictional claims in published maps and institutional affiliations.

Springer Nature or its licensor (e.g. a society or other partner) holds exclusive rights to this article under a publishing agreement with the author(s) or other rightsholder(s); author self-archiving of the accepted manuscript version of this article is solely governed by the terms of such publishing agreement and applicable law.